Silicon (2022) 14:5961–5973
https://doi.org/10.1007/s12633-021-01322-x

ORIGINAL PAPER

Breakdown Voltage Enhancement of $Al_{0.1}Ga_{0.9}$ N Channel HEMT with Recessed Floating Field Plate

Ramkumar Natarajan[1] · Eswaran Parthasarathy[1]

Received: 12 July 2021 / Accepted: 9 August 2021 / Published online: 13 September 2021
© Springer Nature B.V. 2021

Abstract

In this paper, electrical and microwave characteristics of $Al_{0.1}Ga_{0.9}$ N channel HEMTs was reported. The device performance were evaluated for conventional gate, field plate gate, and recessed floating field plate with Silicon nitride (SiN)/Hafnium oxide (HfO_2) passivation. The recessed floating field plate HEMT with gate length $L_G = 0.8$ μm, gate to drain distance $L_{GD} = 1$ μm, and HfO_2 (SiN) passivation HEMT reports peak drain current density (I_{DS}) of 0.282(0.288) A/mm at $V_{GS} = 0$ V, three terminal off-state breakdown voltage (V_{BR}) of 677 (617) V, 6.38 Ω.mm of ON-resistance (R_{ON}), transconductance ($g_{m,max}$) of 93(95) mS/mm, and F_T/F_{MAX} of 11.4/49 (12/22) GHz. The HfO_2 (SiN) passivation device demonstrated the Johnson figure of merit (JFoM)) of 7.71 (7.404) THz.V and F_{MAX} x V_{BR} product of 33.173 (13.574) THz.V. The high JFoM along with high F_{MAX} x V_{BR} indicates the potential of the ultrawide bandgap AlGaN HEMTs for future power switching and high-power microwave applications. The breakdown voltage (V_{BR}) of the floating field plate HEMT is improved 54 % from conventional HEMT and 31 % improvement from gate field plate HEMT.

Keywords Floating Field plate · breakdown voltage · electric field · high power applications · HEMTs

1 Introduction

Group III-nitride based wide-bandgap semiconductors are used in high power microwave and switching applications. Owing the unique combination of high electron density, higher mobility, and high critical electic field of conventional GaN channel-based high electron mobility transistors enables high power and high frequency operation for the past two decades [1–4] and GaN based based power switches, RF amplifiers, and power diodes are commercially available in the market from multiple vendor [5]. Moreover, GaN-HEMTs are widely used in low-noise microwave applications due to its excellent noise performance [6–8]. On other hand, AlGaN ternary channel-based HEMTs are also an interesting devices alternate to GaN-channel HEMTs interms of high breakdown voltage due to ultrawide bandgap features of AlGaN material. AlGaN channel based HEMTs had proven its potential for fast-switching and low switching loss applications, particularly in high temperature and high radiation environments [9–29]. Existence of large critical electrical field (> 3.3 MV/cm) and on par with GaN saturation velocity [30], the AlGaN channel based HEMTs are recognized as the most optimistics candidates future high-power switching as well as microwave applications in harsh environments [31].

After the first successful demonstartion of AlGaN channel based HEMT for high power and microwave application [10], several research groups reported the high performance of AlGaN channel HEMTs. T. Nanjo et.al. investigated the HEMT on AlN buffer and the device shown enrich V_{BR} by suppressing the drain leakage current [11]. Takuma Nanjo et al. reported the ternary channel (AlGaN) HEMT on sapphire, the breakdown voltage of 1700 V for L_{GD} of 10 μm [12]. Sanyam Bajaj et al. reported $Al_{0.75}Ga_{0.25}$ N channel HEMT with reduce source/drain contact resistances by n + + AlGaN region [13]. The 20 nm Al_2O_3 gate dielectric MISFETs demonstrated 14 mS/mm of $g_{m,\ max}$ and 224 V of breakdown voltage (V_{BR}). Albert G. Baca et al. demonstrated a circular HEMT with a V_{BR} of 810 V for 2.0 μm gate length and 314 μm circumference [14]. SakibMuhtadi et al. revealed high Al-content AlGaN channel HEMTs on AlN buffer and the device shown better thermal conduction. Operated up to 40 V at 0.25 A/mm without current collapse [15]. A high breakdown voltage of 2200 V was attained for 22 μm gate to drain

✉ Eswaran Parthasarathy
eswaranp@srmist.edu.in

[1] Department of Electronics and Communication Engineering, SRM Institute of Technology and Sciences, Chennai, India

distance device by adopting ohmic/Schottky-hybrid drain contacts [16]. Ming Xiao et al. reported GaN/$Al_{0.35}Ga_{0.65}$ N/AlN/graded channel HEMT and the device shown enhanced I_{DS} and high I_{on}/I_{off} ratio with improved breakdown voltage [17]. The first RF performance on AlGaN channel based HEMT was reported byAlbert G. Baca et.al. An 80 nm gate length HEMT yields I_{DS} of 0.16 A/mm, and 24 mS/mm of $g_{m,max}$, and having F_T/F_{MAX} of 28.4/18.5 GHz [18]. An RF simulation study on AlGaN HEMT channel based HEMTs reported its potential for large signal RF application as well as power switching applications [24]. Zhang et al. proposed AlGaN double channel HEMTs for improving carrier transport and 2DEG density [27], however the large negative threshold voltage of the device may result in off-state power loss.

The bandgap of the $Al_xGa_{1-x}N$ tailoring by varying the Al composition ($0 < x < 1$).The high critical breakdown field and low on resistance (R_{ON}) are key parameters for power switching applications. Lateral Figure of Merit (LFOM)is used to estimate the potential of a material for power switching [32];

$$LFOM = \frac{V_B^2}{R_{on}} = q\mu_{ch} n_s E_C^2 \tag{1}$$

The LFOM of a material depends on the sheet charge density (n_s), critical electric field (E_c), and mobility of the channel (μ_{ch}). Since the critical electric field of AlGaN channel is higher $\left(E_c \sim E_g^n, 2 < n < 2.5\right)$ than the GaN channel, $Al_xGa_{1-x}N$ channel offers significant improvement in V_{BR} even at high temperature over GaN. The JFOM measures the ability of the materials for high power microwave applications;

$$JFOM = V_B.F_T = \frac{E_c \nu_{sat}}{2\pi} \tag{2}$$

The JFOM of material systems is the product of F_T and V_{BR}. The critical electric field (E_c), and electron saturation velocity (ν_{sat}) influences the JFOM of the HEMT. Since the low Al composition $Al_xGa_{1-x}N$ channel saturation velocity is on par with GaN channel, along with enhanced critical field improves the JFOM of AlGaN channel HEMTs than GaN-based HEMTs. The high V_{BR} is achieved for long channel L_G, long L_{GD} HEMTs, along with Al-richAlGaN channel [9–29]. Whereas, the smaller L_G,L_{GD}, and low Al composition of AlGaN channel results in improved cut-off frequency with the suppressed V_{BR} and hence, there is a trade-off between V_{BR} and device speed (cut-off frequency) of HEMTs.

In this work, we proposed the recessed floating field plate, $Al_{0.1}Ga_{0.9}$ N channel HEMT for improve the V_{BR} of the device with satisfactory RF performance. $L_G = 0.8$ μm, and $L_{GD} = 1$ μm $Al_{0.31}Ga_{0.69}$ N/$Al_{0.1}Ga_{0.9}$ N HEMT on sapphire substrate is investigated using Silvaco ATLAS TCAD numerical simulation for SiN and HfO_2 passivation.

The HfO_2 passivation device shown remarkable improvement in breakdown voltage than SiN passivation. The organization of this work as follows; Device structure description for conventional gate HEMT (Device A), Gate field plate HEMT (Device B), and recessed floating field plate HEMTs (Device C) is discussed in Sec. 2. The physics-based simulation models are described in Sec. 3. The DC and microwave characteristic of proposed HEMT with experimental validation is discussed in Sec. 4 with concluding remarks.

2 Device Structure Description

The $Al_{0.1}Ga_{0.9}$ N channel geometry of conventional gate HEMT (Device A), Gate field plate HEMT (Device B), and recessed floating field plate HEMTs (Device C) are displayed in Fig. 1(a), (b), and (c) respectively. The device grown on sapphire substrate and consists of 23 nm $Al_{0.31}Ga_{0.69}$ N barrier (E_g ~ 3.989 eV), 100 nm $Al_{0.1}Ga_{0.9}$ N channel (E_g ~ 3.563 eV), and 2.2 μm buffer. The device DC and RF performance are evaluated for 100 nm SiN and HfO_2 passivation. High Al composition in the $Al_xGa_{1-x}N$ channel attenuates the mobility of the device [30] and also a very low Al composition in the $Al_xGa_{1-x}N$ channel degrades the breakdown voltage of the device. Therefore, we have used the optimum value of Al composition to balance the mobility as well as breakdown voltage of the HEMT. The model device used in simulation has a 0.8 μm gate length, 1 μm gate to drain distance, and 0.8 μm gate to source distance. The source and drain ohmic contacts are realized by setting the work function of the source/drain electrode to 3.4 eV and Schottky contact was made by setting the gate electrode work function as 5.2 eV for the TCAD simulation. The conduction band offset along with interface charge details of the heterostructure shown in Fig. 2. At room temperature TCAD simulation exhibited 1.01×10^{13} $cm^{-2}$of electron density and 810 cm^2V^{-1} s^{-1} of carrier mobility in the 2DEG.

3 Simulation Models

The proposed HEMTis analyse during several device physics models in TCAD simulation including mobility model, recombination models, carrier transport, and polarization models.

Polarization charge at the heterostructure interface is as follows [33];

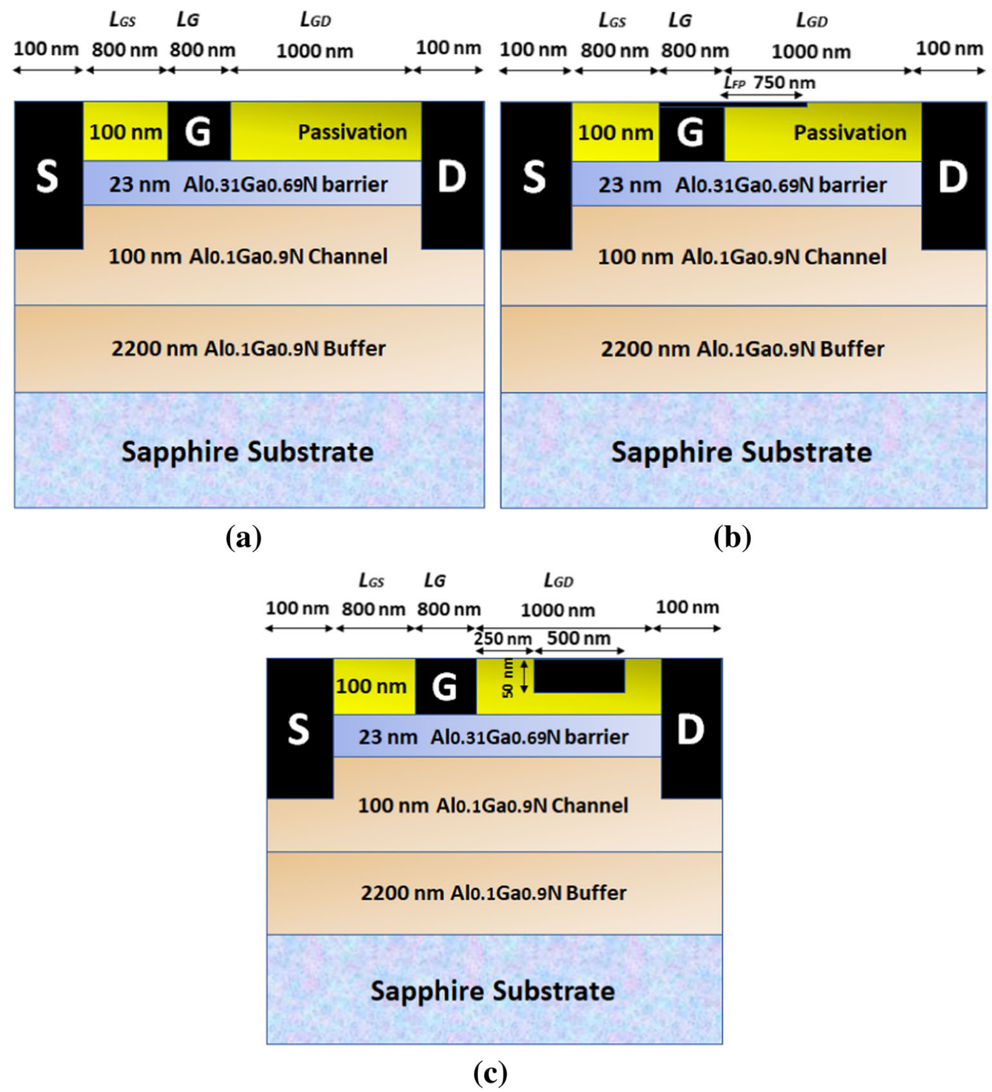

Fig. 1 Structure of $Al_{0.1}Ga_{0.9}$ N channels (**a**) conventional HEMT (Device A), (**b**) Gate field plate (Device B), (**c**) Recessed floating field plate (Device C)

$$P_{total} = [P_{PE}(bottom) + P_{SP}(bottom)] - [P_{PE}(top) + P_{SP}(top),] \tag{3}$$

The P_{total} at the top/bottom heterointerface depends on the spontaneous (P_{SP}) and piezoelectric polarization (P_{PE}) of the materials. The temperature dependent mobility model $\mu_0(T,N)$ describes as following form [30];

$$\mu_0(T,N) = \mu^{\beta_1}_{\min\left(\frac{T}{300}\right)} + \frac{(\mu_{max} - \mu_{min})\left(\frac{T}{300}\right)^{\beta_2}}{1 + \left[\frac{N}{N_{ref}\left(\frac{T}{300}\right)^{\beta_3}}\right]^{\alpha\left(\frac{T}{300}\right)^{\beta_4}}} \tag{4}$$

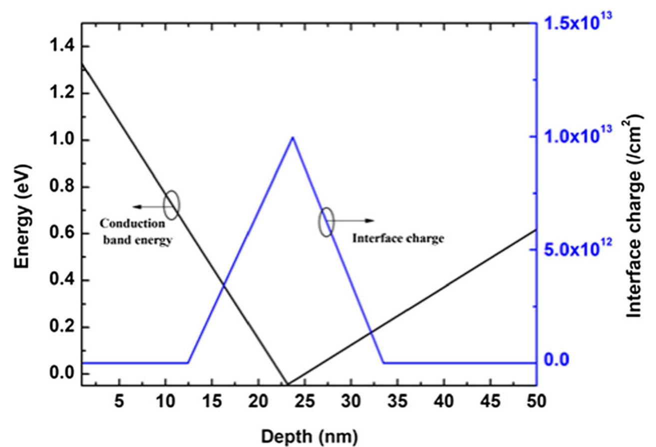

Fig. 2 Conduction band and interface charge diagram of $Al_{0.31}Ga_{0.69}$ N/ $Al_{0.1}Ga_{0.9}$ N heterostructure

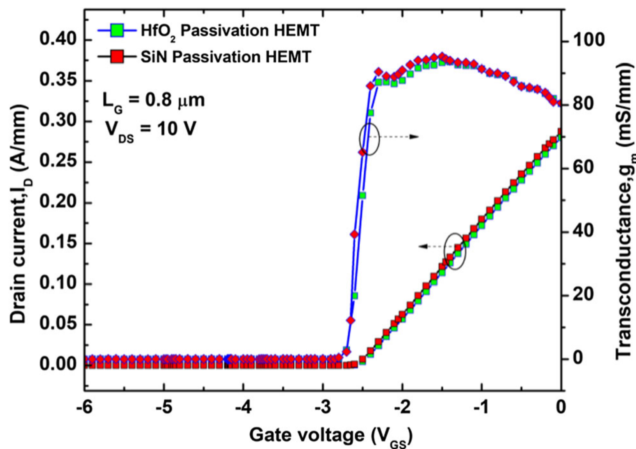

Fig. 3 Transfer characteristics of recessed floating gate HEMT (Device C)

The capture of phonon transition within the forbidden bandgap due to trap states, Shockley-Read-Hall (SRH) recombination model is used. The SRH model expresses as a function of electron life time τ_n and holes life time τ_p, temperature, trap energy level E_{trap} [34];

$$R_{net}^{SRH} = \frac{n - n_{ie}^2}{\tau_p\left[p + n_{ie}\exp\left(\frac{-E_{trap}}{KT}\right)\right] + \tau_n\left[p + n_{ie}\exp\left(\frac{-E_{trap}}{KT}\right)\right]}, \quad (5)$$

The Selberherr's impact ionization model considered for device breakdown simulation [35] and the impact ionization carrier generation rate described as follows:

$$G = \left(\alpha_n|J_p| + a_p|J_p|\right)/q \quad (6)$$

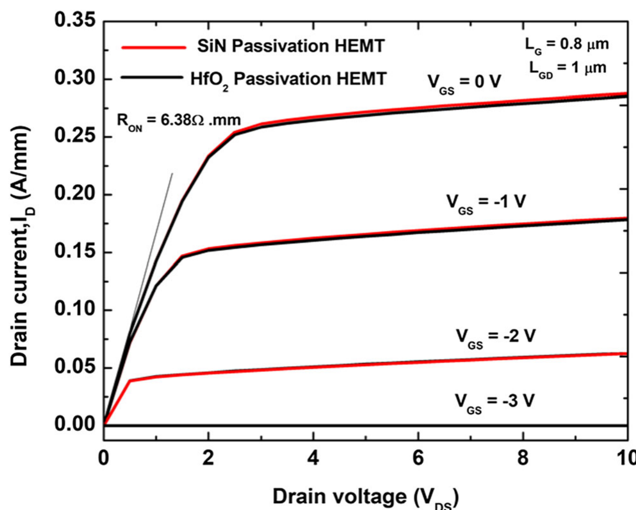

Fig. 4 I - V characteristics of recessed floating gate HEMT (Device C)

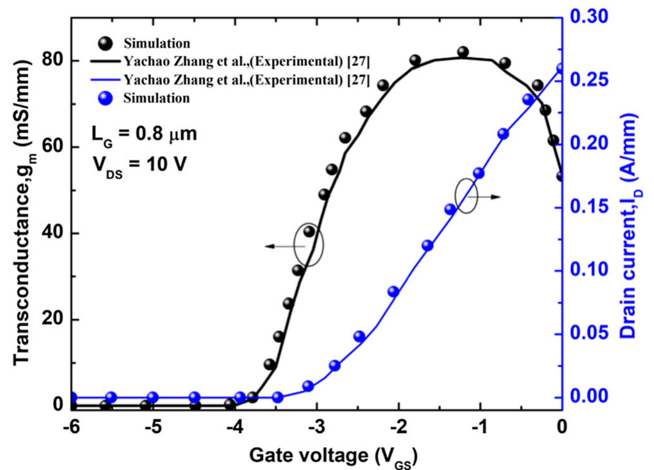

Fig. 5 Transfer characteristics for $L_G = 0.8$ μm of $Al_{0.1}Ga_{0.9}$ N channel HEMT (Device C) and experimental work [27]

Where, E is the electric field, electrons ionization rate $\alpha_n = A_n exp(-B_n)/|E|$ and holes ionization rate $\alpha_p = A_p exp(-B_p)/|E|$. The fitting parameters A_n, A_p, B_n, and B_p values are taken from [34] for the simulation.

4 Results and Discussions

The proposed recessed floating gate HEMT (Device C) transfer characteristic is depicted in Fig. 3 for $V_{DS} = 10$ V and V_{GS} swept from − 6 to 0 V. The conventional and gate field plate HEMTs also exhibited similar response. $Al_{0.1}Ga_{0.9}$ N HEMT with $L_G = 0.8$ μm has reached the maximum output current (I_{DS}) of 0.28 A/mm and $g_{m,max}$ of 95 mS/mm. The threshold voltage (V_{th}) of the HEMT is extracted as -3 V. The V_{th} of the

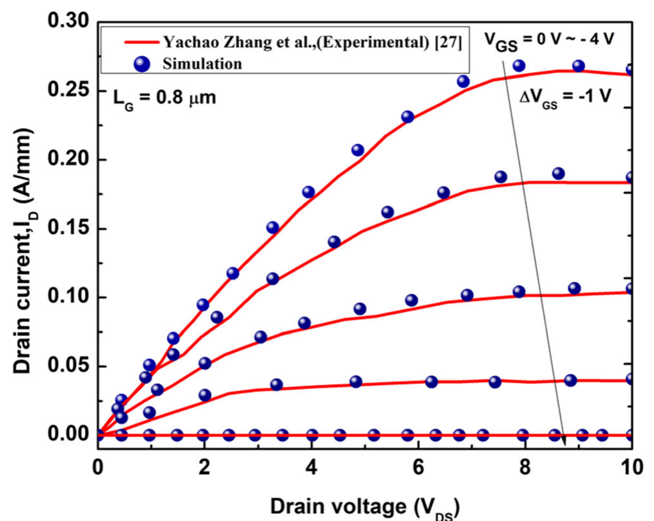

Fig. 6 Output characteristics for $L_G = 0.8$ μm of $Al_{0.1}Ga_{0.9}$ N channel HEMT (Device C) and experimental work [27]

Fig. 7 E-field distribution for SiN passivation of (**a**) Device A (**b**) Device B (**c**) Device C

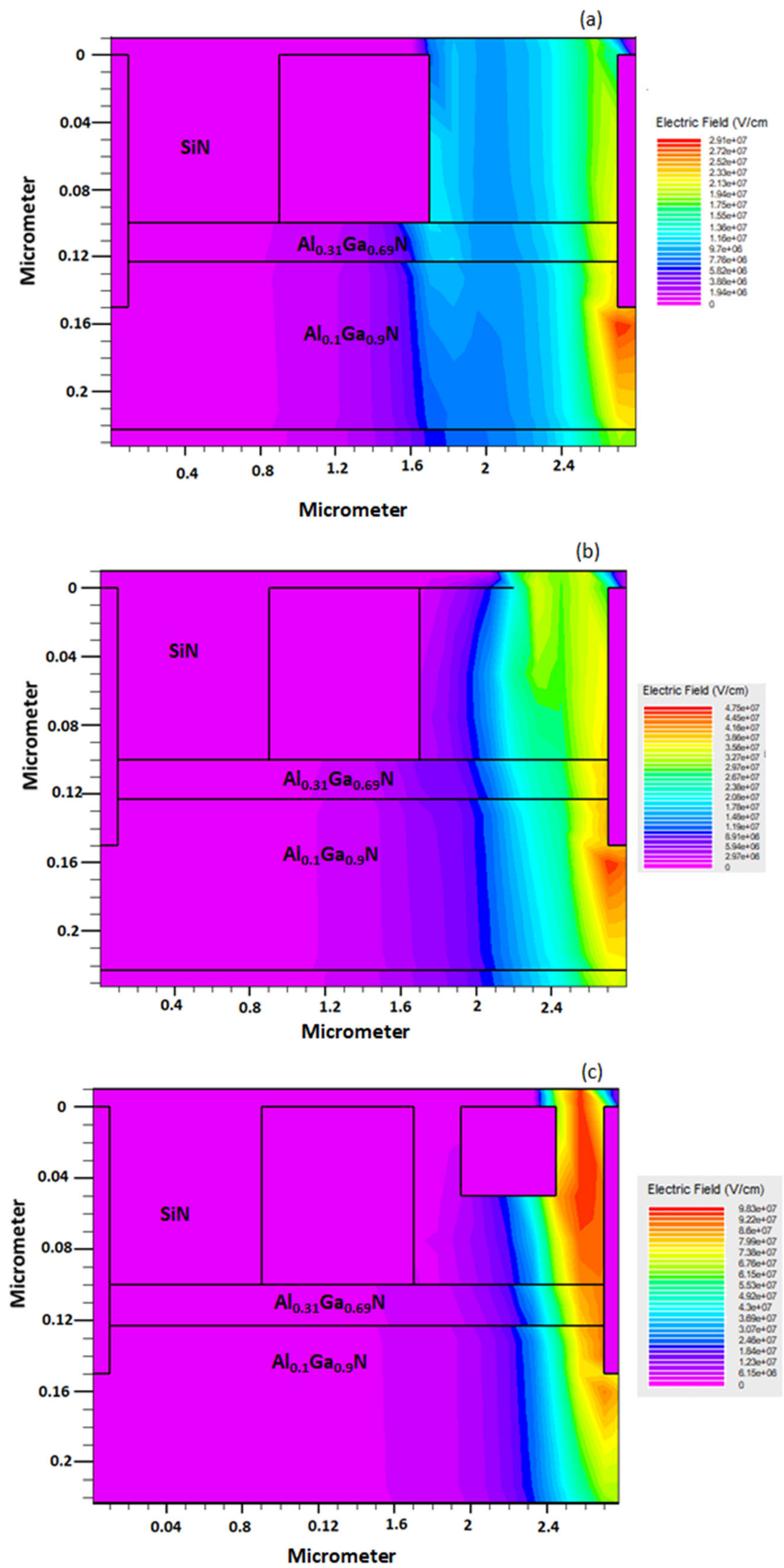

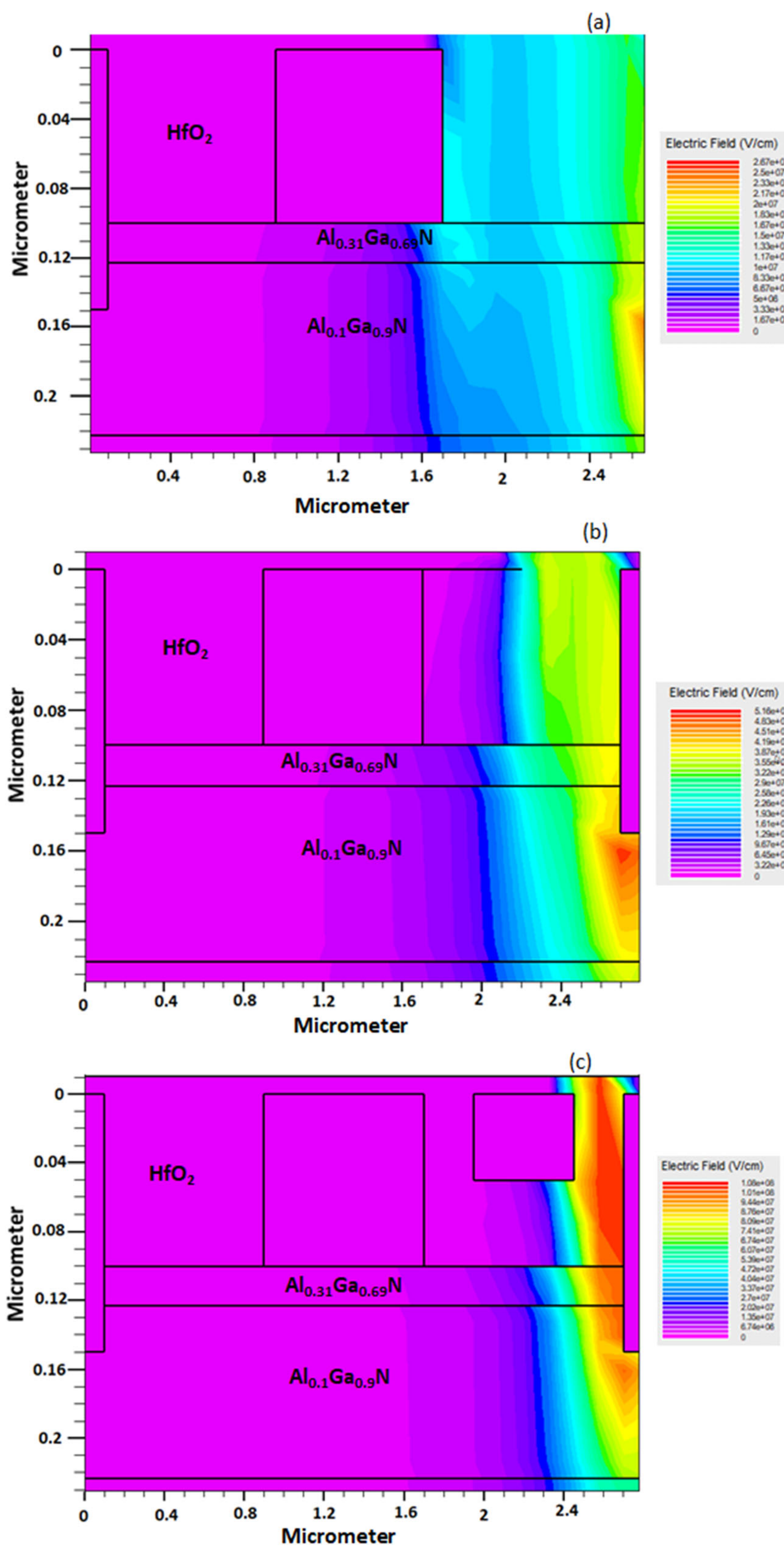

Fig. 8 E-field distribution for HfO_2 passivation of (**a**) Device A, (**b**) Device B and (**c**) Device C

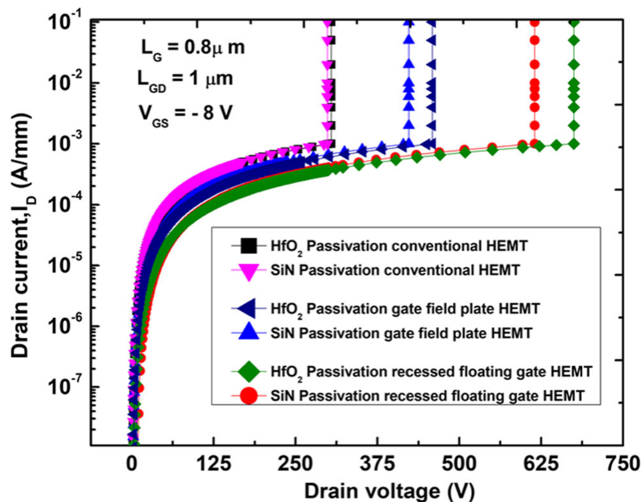

Fig. 9 Off-state breakdown characteristics of L_G = 0.8 μm $Al_{0.1}Ga_{0.9}$ N channel HEMTs

HEMT obtained from V_{GS} intercepted of the linear extrapolation in the active region.The V-I characteristics of the proposed Device C is shown in Fig. 4 for V_{GS} = -3 to 0 V and V_{DS} swept from 0 V to 10 V. Device A and Device B also exhibited similar output characteristics. The extracted ON-resistance (R_{ON}) of the device from the V-I characteristics (V_{GS} = 0 V) is 6.38 Ω.mm. The R_{on} resistance of the device extracted from the output characteristics at V_{GS} = 0 V By taking the slope (1/Ron = I_{DS}/ V_{DS}) corresponding to ¼ th of maximum drain current ($I_{DS,\ max}$). The device is perfectly pinched-off at V_{GS} = -3 V. The proposed device R_{ON} resistance is comparatively lower than the reported works [10–28]. The transfer and output characteristics of simulation result of conventional $Al_{0.1}Ga_{0.9}$ N channel HEMT is validated with experiment result of [27] and it is shown in Figs. 5 and 6 respectively. The simulated results were well correlated with the reported experimental work.

The HEMT breakdown simulation was carried out at off-state condition (V_{GS} = -8 V). The electric field (E-filed) distributions for SiN and HfO_2 passivation of (a) Device A, (b) Device B and (c) Device C are depicted in Figs. 7 and 8 respectively. The permittivity (ε_r) and thickness (t) of the insulator (passivation) modulates the E-field. High permittivity HfO_2 (ε_r=25) passivation smoothening the E-filed at gate and drain edge [35–38].

From Fig. 7(a) (SiN passivation) and Fig. 8(a) (HfO_2 passivation), it is observed that a peak E-field exist at the gate edge, which lower the V_{BR} of the device. Therefore, sinking the field distribution becomes the alternate solution to enhance the V_{BR}. In general, the gate field plate (FPs), source field plate (SFPs), and drain connected field plate techniques are used to suppress the electric field [39]. The gate field plate techniques demonstarted the improved breakdown voltage by alleviating high E-field as shown in Fig. 7(b) (SiN passivation) and Fig. 8(b) (HfO_2 passivation) and it reshaping the field distribution.

In this work, a recessed floating field plate structure is considered for further, to enhance the breakdown voltage of the HEMTs. The electic field distribution of proposed HEMTs are shown in Fig. 7(c) (SiN passivation) and Fig. 8(c) (HfO_2 passivation).

The introduction of floating field plate, reshaped the electric field and suppressed the E-field near the gate edge effectively and a peak electric field found at the drain side edge of the floating field plate because of much closer with drain electrode and also the recessed field plate is very closer with 2DEG channel than gate field plate results in better surface field distribution, which enhances the breakdown voltage of the HEMTs. The E-field engineering soley depends on field plate length, passivation permittivity, thickness of the passivation, and recess depth.

For the proposed Device C dimensions, the off-state breakdown voltage characteristics of HEMTs are plotted in Fig. 9. The breakdown voltage of the HEMT extracted from I_D-V_D curves at the intersection of the extrapolated saturation segment (an V_D saturated and a sudden increase in I_D). The recessed floating field plate HEMT shown remarkable V_{BR} of 677 (617) V for HfO_2 (SiN) passivation. However, the conventional HEMT shown V_{BR} of 307(297) V and gate filed plate shown V_{BR} of 462 (428) V. From this analysis of off state breakdown voltage simulation, the floating field plate demonstared 54 % improvement in V_{BR} than conventional HEMT, and 31 % higher than the gate field plate HEMT.

The Figs. 10 and 11 shows the simulation results of electron concentration distribution of HEMTs at breakdown condition. The larger depletion region of floating field plate shown in Figs. 10(c) and 11(c), suppressed E-field near the drain side of gate edge, and high critical field of $Al_{0.1}Ga_{0.9}$ N channel are the major reason for improving the breakdown voltage of the proposed HEMTs.

The microwave performance of the SiN and HfO_2 passivated Device C are depicted in Figs. 12 and 13 respectively. The F_T/F_{MAX} of the device extracted from current gain and power gain when it reaches 0 dB respectively. The conventional HEMTs are showing better F_T than field plated HEMTs. Due to the introduction of additional field plate in the device structure,increases the parasitic capacitance (C_{GS} and C_{GD}) which limits the speed of the HEMTs as given in the Eqs. (9);

$$P_{RF} == \frac{I_{max}[V_{br} - V_{knee}]}{8}, \quad (7)$$

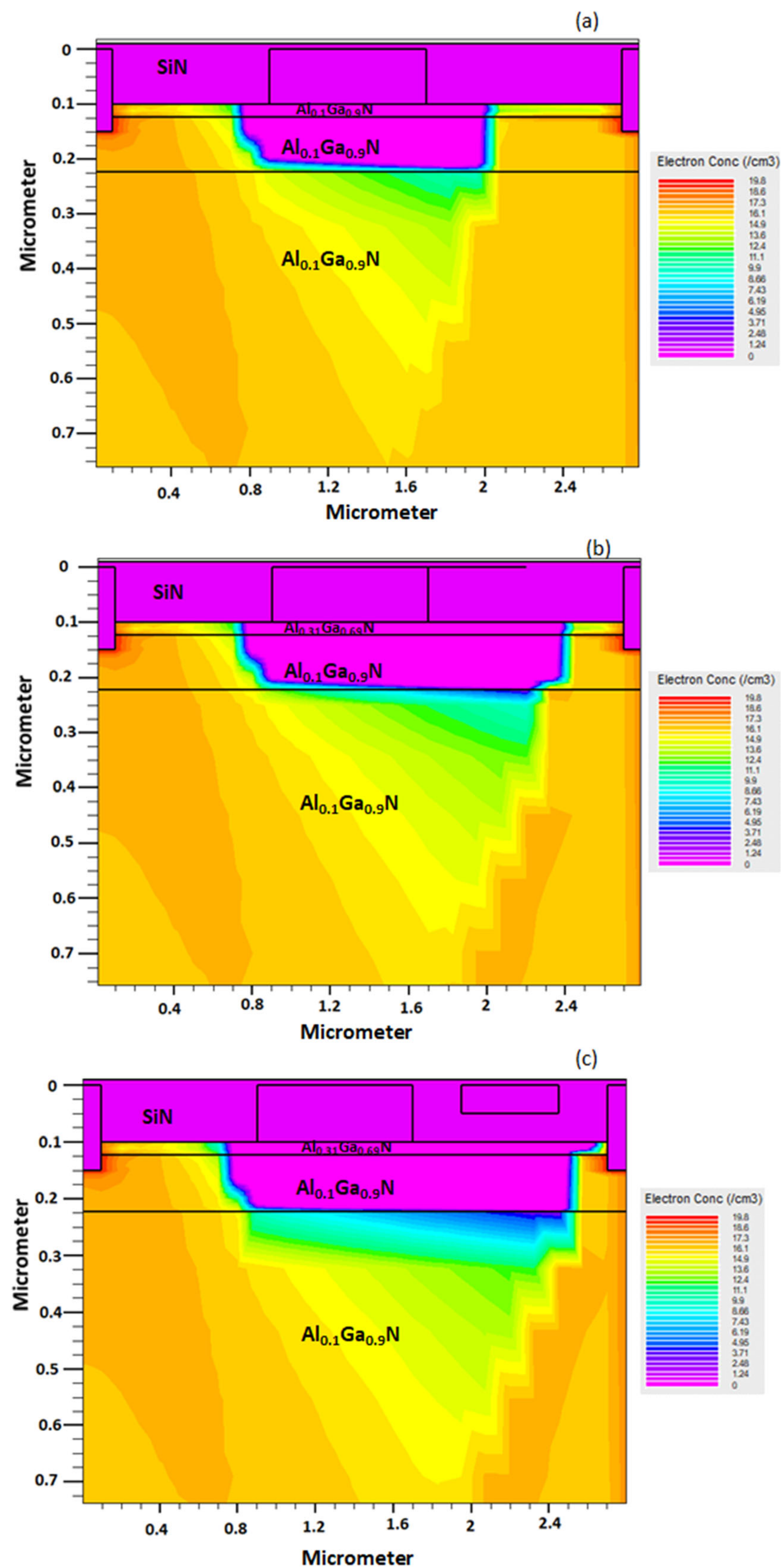

Fig. 10 Electron concentration distribution of SiN passivation (**a**) Device A, (**b**) Device B and (**c**) Device C at breakdown voltage condition

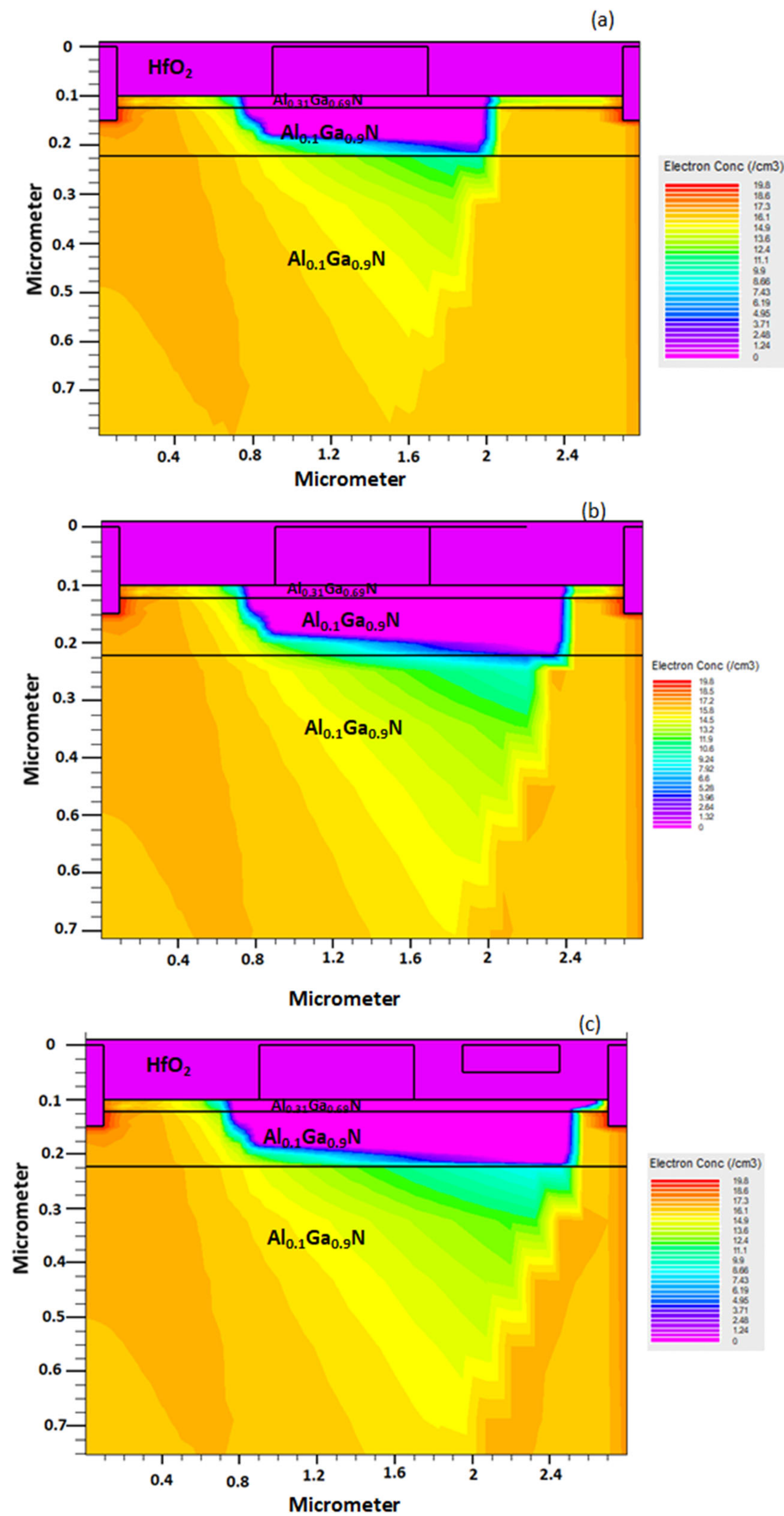

Fig. 11 Electron concentration distribution of HfO_2 passivation (**a**) Device A, (**b**) Device B and (**c**) Device C at breakdown voltage condition

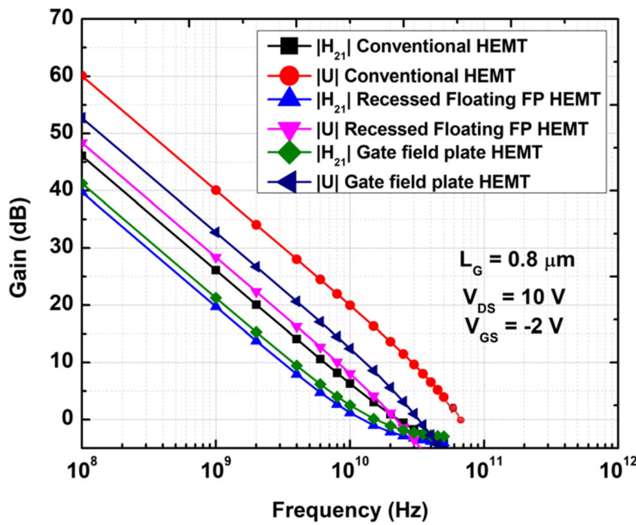

Fig. 12 Microwave performance of SiN passivation HEMTs

$$F_T = \frac{G_m}{2\pi(c_{Gs} + c_{GD})}, \quad (8)$$

$$F_{MAX} = \frac{F_T}{\sqrt{(R_i + R_s + R_g)g_0 + (2\pi F_T)R_G C_{GD}}}, \quad (9)$$

The I_{DS} and $V_{BR}$of a transistor expected to be very high for delivering high RF output power density as shown in Eq. (8). The proposed recessed floating field plate HEMT shown a F_T/F_{MAX} of 11.4/49 GHz for HfO2 passivation and 12/22 GHz for SiN passivation. The improved power performance along with the satisfactory cut-off frequencyof the proposed HEMTs demonstrated its capability for future RF and power switching applications. Further the small signal RF charcateristics can be enhanced by scale down the device dimensions.

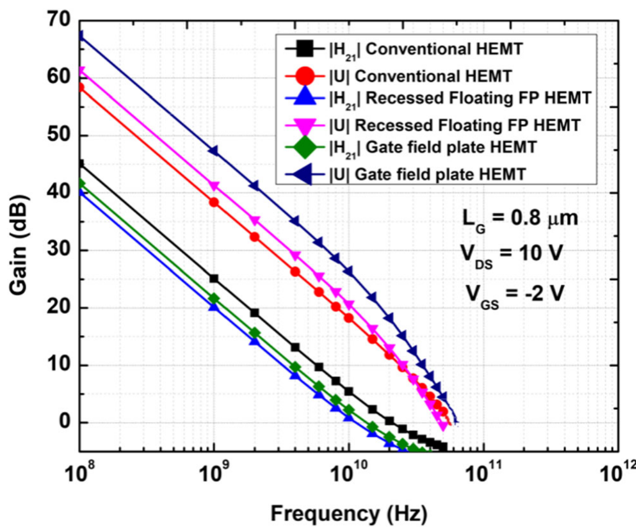

Fig. 13 Microwave performance of HfO_2 passivation HEMTs

Table. 1 State of art AlGaN channel parameter and performance

Author, Year	Reference No	Gate length (L_G)	Gate to drain distance (L_{GD})	Drain current (I_{DS})	Breakdown voltage (V_{BR})	Cut-off frequency (F_T/F_{MAX})	JFoM (THz.V)
V. Adivarahan et al., 2008	[10]	1 μm	3 μm	0.11 A/mm	463 V	-	-
T. Nanjo et al., 2009	[11]	1 μm	2 μm	0.14 A/mm	350 V	-	-
Takuma Nanjo et al., 2013	[12]	1 μm	3 μm	0.18 A/mm	500 V	-	-
Sanyam Bajaj et al., 2016	[13]	0.7 μm	1.1 μm	0.05 A/mm	224 V	-	-
Albert G. Baca et al., 2016	[14]	2 μm	10 μm	-	810 V	-	-
W. Zhang et al., 2018	[16]	3 μm	6 μm	-	500 V		-
Ming Xiao et al., 2018	[17]	1 μm	5 μm	0.3 A/mm	408 V		-
Albert G. Baca et al., 2018	[18]	80 nm	0.5 μm	0.1 A/mm	92 V	28.4/18.5 GHz	2.6128
Andrew M. Armstrong et al., 2019	[19]	3 μm	2.7 μm	0.1 A/mm	620 V	-	-
HaoXue et al., 2019	[20]	160 nm	0.6 μm	0.42 A/mm	170 V	20/40 GHz	3.4
Yachao Zhang et al., 2020	[27]	0.8 μm	1 μm	0.24 A/mm	143 V	-	-
Shahadat H. Sohel et al., 2020	[28]	0.7 μm	3.5 μm	0.3 A/mm	125 V	14/22 GHz	1.75
This work (SiN Passivation)		0.8 μm	1 μm	0.288 A/mm	617 V	12/22 GHz	7.4
This work (HfO2 Passivation)		0.8 μm	1 μm	0.282 A/mm	677 V	11.4/49 GHz	7.718

The comparison of state of art AlGaN channel based HEMTs parameter and performance along with proposed Device C are tabulated in Table 1. The proposed Device C shows improved drain current, breakdown volatge, and RF perfomance among the reported work for L_{GD} (1 μm) and L_G(0.8 μm).

5 Conclusions

Breakdown voltage performance analysis of $Al_{0.1}Ga_{0.9}$ N channel HEMT is reported with floating field plate and AlGaN buffer. A Physics-based Technology Computer Aided Design(TCAD) simulation results shows that the peak electric field near the drain-side of gate edge is majorly reduced by recessed floating filed plate technique, which further elevated the breakdown performance of the AlGaN channel HEMTs. The insertion of floating filed plate reshaped the E-field distribution in the access region effectively and reduced the E-field near the drain side of gate edge and thus enhanced the breakdown voltage. The proposed recessed floating field plate HEMT yields V_{BR} of 677 Vand F_T/F_{max}11.4/49 GHz for a high-k HfO_2 passivation. The breakdown voltage (V_{BR}) of the HfO_2 passivation floating field plate HEMT is improved 54 % from conventional HEMT and 31 % improvement from gate field plate HEMT. The excellent breakdown power performances along with RF characteristics of the ultrawide bandgap AlGaN channel based HEMTs are attractive alternate devices for next geneartion power electronics and RF applications.

Acknowledgements The authors acknowledge the Department of Electronics and Communication Engineering, SRM Institute of Science and Technology, Chennai, India for research facility and support to carry out this research work.

Authors' Contributions All the works reported in this paper is original and have done with equal contribution in all the sections by Ramkumar Natarajan and Eswaran Parthasarathy.

Data Availability Not Applicable.

Code Availability Not Applicable.

Declarations

Manuscripts is prepared strictly adhering to the norm of the journal, contains 5 Sections and no sub sections.

Ethics Approval Not Applicable.

Consent to Participate Not Applicable.

Conflicts of Interest/Competing Interests The authors declare that there is no conflict of interest reported in this paper.

Consent for Publication Not applicable as the manuscript does not contain any data from individual.

Disclosure of Potential Conflicts of Interest Not Applicable.

Research Involving Human Participants and/or Animals Not Applicable.

Informed Consent Not Applicable.

References

1. Zeng F, An JX, Zhou G, Li W, Wang H, Duan T, Jiang L, Yu H (2018) A comprehensive review of recent progress on GaN high electron mobility transistors: devices, fabrication and reliability. Electronics 7:377. https://doi.org/10.3390/electronics7120377
2. Roccaforte F, Fiorenza P, Greco G, Nigro RL, Giannazzo F, Iucolano F, Saggio M (2018) Emerging trends in wide band gap semiconductors (SiC and GaN) technology for power devices. Microelectron Eng 187–188:66–77. https://doi.org/10.1016/j.mee.2017.11.021
3. Husna Hamza K, Nirmal D (2020) A review of GaN HEMT broad-band power amplifiers, AEU. Int J Electron Commun 116:153040. https://doi.org/10.1016/j.aeue.2019.153040
4. Ma C-T, Gu Z-H (2019) Review of GaN HEMT applications in power converters over 500 W. Electronics 8(12):1401. https://doi.org/10.3390/electronics8121401
5. Flack TJ, Pushpakaran BN, Bayne SB (2016) GaN technology for power electronic applications: a review. J Electron Mater 45:2673–2682. https://doi.org/10.1007/s11664-016-4435-3
6. Tong X, Zhang S, Xu J, Zheng P, Shi X, Huang Y, Wang Q (2018) 18-31 GHz GaN wideband low noise amplifier (LNA) using a 0.1 μm T-gate high electron mobility transistor (HEMT) process. Int J RF Microwave Comput Aided Eng 28:e21425. https://doi.org/10.1002/mmce.21425
7. Jarndal A, Hussein A, Crupi G, Caddemi A (2020) Reliable noise modeling of GaN HEMTs for designing low-noise-amplifiers. IJNM 33:e2585. https://doi.org/10.1002/jnm.2585
8. Nalli A, Raffo A, Crupi G, D'Angelo S, Resca D, Scappaviva F, Salvo G, Caddemi A, Vannini G (2015) GaN HEMT noise model based on electromagnetic simulations. IEEE Trans Microw Theory Tech 63:2498–2508. https://doi.org/10.1109/TMTT.2015.2447542
9. Nanjo T, Takeuchi M, Suita M, Abe Y, Oishi T, Tokuda Y, Aoyagi Y (2007) First operation of AlGaN channel high electron mobility transistors. Appl Phys Express 1:011101. https://doi.org/10.1143/APEX.1.011101
10. Nanjo T, Takeuchi M, Suita M, Oishi T, Abe Y, Tokuda Y, Aoyagi Y (2008) Remarkable breakdown voltage enhancement in AlGaN channel high electron mobility transistors. Appl Phys Lett. 92:263502. https://doi.org/10.1063/1.2949087
11. Nanjo T, Takeuchi M, Imai A, Suita M, Oishi T, Abe Y, Yagyu E, Kurata T, Tokuda Y, Aoyagi Y (2009) AlGaN channel HEMTs on AlN buffer layer with sufficiently low off-state drain leakage current. Electron Lett 45:1346–1348. https://doi.org/10.1049/el.2009.2711
12. Nanjo T, Imai A, Suzuki Y, Abe Y, Oishi T, Suita M, Yagyu E, Tokuda Y (2013) AlGaN channel HEMT with extremely high breakdown voltage. IEEE Trans Electron Devices 60:1046–1053. https://doi.org/10.1109/TED.2012.2233742

13. Bajaj S, Akyol F, Krishnamoorthy S, Zhang Y, Rajan S (2016) AlGaN channel field effect transistors with graded heterostructure ohmic contacts. Appl Phys Lett 109:133508. https://doi.org/10.1063/1.4963860
14. Baca AG, Armstrong AM, Allerman AA, Douglas EA, Sanchez CA, King MP, Coltrin ME, Fortune TR, Kaplar RJ (2016) An AlN/Al0.85Ga0.15N high electron mobility transistor. Appl Phys Lett 109:033509. https://doi.org/10.1063/1.4959179
15. Sakib Muhtadi; Seong Mo Hwang MVS Chandrashekhar; Asif Khan(2017) Antwon Coleman;Fatima Asif;Grigory Simin10.1109/LED.2017.2701651Muhtadi S, Hwang SM, Coleman A, Asif F, Simin G, Chandrashekhar MVS, Khan A (2017) High electron mobility transistors with Al0.65Ga0.35N channel layers on thick AlN/sapphire templates. IEEE Electron Device Lett 38:914–917. https://doi.org/10.1109/LED.2017.2701651
16. Zhang W, Zhang J, Xiao M, Zhang L, Hao Y (2018) High breakdown-voltage (> 2200 V) AlGaN-channel HEMTs with ohmic/schottky hybrid drains. IEEE J Electron Devices Soc 6:931–935. https://doi.org/10.1109/JEDS.2018.2864720
17. Xiao M, Zhang J, Duan X, Zhang W, Shan H, Ning J, Hao Y (2018) High performance Al0.10Ga0.90N Channel HEMTs. IEEE Electron Device Lett 39:1149–1151. https://doi.org/10.1109/LED.2018.2848661
18. Baca AG, Klein BA, Wendt JR, Lepkowski SM, Nordquist CD, Armstron AM, Allerman AA, Douglas EA, Kaplar RJ (2019) RF performance of Al0.85Ga0.15N/Al0.70Ga0.30N high electron mobility transistors with 80-nm gates. IEEE Electron Device Lett 40:17–20. https://doi.org/10.1109/LED.2018.2880429
19. Armstrong AM, Klein BA, Baca AG, Allerman AA, Douglas EA, Colon A, Abate VM, Fortune TR (2019) AlGaN polarization-doped field effect transistor with compositionally graded channel from $Al_{0.6}Ga_{0.4}N$ to AlN. Appl Phys Lett 114:052103. https://doi.org/10.1063/1.5058263
20. Xue H, Hwang S, Razzak T, Lee C, Ortiz GC, Xia Z, Sohel SH, Hwang J, Rajan S, Khan A, Lu W (2020) All MOCVD grown Al0.7Ga0.3N/Al0.5Ga0.5N HFET: An approach to make ohmic contacts to Al-rich AlGaN channel transistors. Solid State Electron 164:107696. https://doi.org/10.1016/j.sse.2019.107696
21. Wang Zhong-Xu, Du Lin, Liu Jun-Wei, Wang Ying, Jiang Yun, Ji Si-Wei, Dong Shi-Wei, Chen Wei-Wei, Tan Xiao-Hong, Li Jin-Long, Li Xiao-Jun, Zhao Sheng-Lei, Zhang Jin-Cheng, Yue Hao (2019) Breakdown voltage enhancement in GaN channel and AlGaN channel HEMTs using large gate metal height. Chin Phys B 29:027301. https://doi.org/10.1088/1674-1056/ab5fb9
22. Mollah S, Gaevski M, Hussain K, Mamun A, Floyd R, Hu X, Chandrashekhar MVS, Simin G, Khan A (2019) Current collapse in high-Al channel AlGaN HFETs. Appl Phys Express 12:074001. https://doi.org/10.7567/1882-0786/ab24b1
23. Erica A. Douglas, Brianna Klein, Andrew A. Allerman, Albert G. Baca, Torben Fortune, Andrew M. Armstrong (2019) Enhancement-mode AlGaN channel high electron mobility transistor enabled by p-AlGaN gate. J Vacuum Sci Technol B 37:021208. https://doi.org/10.1116/1.5066327
24. Reza S, Klein BA, Baca AG, Armstrong AM, Allerman AA, Douglas EA, Kaplar RJ (2019) High-frequency, high-power performance of AlGaN-channel high-electron-mobility transistors: an RF simulation study. Jpn J Appl Phys 58:SCCD04. https://doi.org/10.7567/1347-4065/ab07a5
25. Wu Y, Zhang J, Zhao S, Zhang W, Zhang Y, Duan X, Chen J, Hao Y (2019) More than 3000 V reverse blocking schottky-drain AlGaN-channel HEMTs with > 230MW/cm2 power figure-of-merit. IEEE Electron Device Lett 40:1724–1727. https://doi.org/10.1109/LED.2019.2941530
26. Xiao M, Zhang W, Zhang Y, Zhou H, Dang K, Zhang J, Hao Y (2019) Novel 2000 V normally-off MOS-HEMTs using AlN/GaN Superlattice channel. 31st International Symposium on Power Semiconductor Devices and ICs (ISPSD), pp 471–474. https://doi.org/10.1109/ISPSD.2019.8757585
27. Zhang Y, Li Y, Wang J, Shen Y, Du L, Li Y, Wang Z, Shengrui U, Zhang J, Hao Y (2020) High-performance AlGaN double channel HEMTs with improved drain current density and high breakdown voltage. Nanoscale Res Lett 15:114. https://doi.org/10.1186/s11671-020-03345-6
28. Shahadat H. Sohel, Andy Xie, Edward Beam, Hao Xue, Towhidur Razzak, Sanyam Bajaj, Sherry Campbell, Donald White, Kenneth Wills, Yu Cao, Wu Lu, Siddharth Rajan (2020), Improved DC-RF dispersion with epitaxial passivation for high linearity graded AlGaN channel field effect transistors. Appl Phys Express 13:036502. https://doi.org/10.35848/1882-0786/ab7480
29. Li L, Yamaguchi R, Wakejima A (2020) Polarization engineering via InAlN/AlGaNheterostructures for demonstration of normally-off AlGaN channel field effect transistors. Appl Phys Lett 117:152108. https://doi.org/10.1063/5.0020359
30. Farahmand M, Garetto C, Bellotti E, Brennan KF, Goano M, Ghillino E, Ghione G, Albrecht JD, Ruden PP (2001) Monte Carlo simulation of electron transport in the III-nitride wurtzite phase materials system: binaries and ternaries. IEEE Trans Electron Devices 48:535–542. https://doi.org/10.1109/16.906448
31. Patrick H. Carey, Fan Ren, Albert G. Baca, Brianna A. Klein, Andrew A. Allerman, Andrew M. Armstrong, Erica A. Douglas, Robert J. Kaplar, Paul G. Kotula, Stephen J. Pearton (2019) Operation up to 500°C of $Al_{0.85}Ga_{0.15}N/Al_{0.7}Ga_{0.3}N$ high electron mobility transistors. IEEE J Electron Devices Soc 7:444–452. https://doi.org/10.1109/JEDS.2019.2907306
32. Coltrin ME, Baca AG, Kaplar RJ (2017) Analysis of 2D transport and performance characteristics for lateral power devices based on AlGaN alloys. ECS J Solid State Sci Technol 6:S3114–S3118. https://doi.org/10.1149/2.0241711jss
33. Ambacher O, Majewski J, Miskys C, Link A, Hermann M, Eickhoff M, Stutzmann M, Bernardini F, Fiorentini V, Tilak V, Schaff B, Eastman LF (2002) Pyroelectric properties of Al(In)GaN/GaN hetero- and quantum well structures. J Phys: Condense Matter 14:3399–3434. https://doi.org/10.1088/0953-8984/14/13/302
34. Int SILVACO. ATLAS User's Manual; Device Simulation Software: Santa Clara, CA, USA, 2016; Available online: https://www.silvaco.com
35. Murugapandiyan P, Hasan MT, Lakshmi VR, Wasim M, Ajayan J, Ramkumar N, Nirmal D (2020) Breakdown voltage enhancement of gate field plate $Al_{0.295}Ga_{0.705}$ N/GaN HEMTs. Int J Electron. https://doi.org/10.1080/00207217.2020.1849819
36. Murugapandiyan P, Nirmal D, Ajayan J, Aarthy Vargheese, Ramkumar N (2021) Investigation of influence of SiN and SiO_2 passivation in gate field plate double heterojunction $Al_{0.3}Ga_{0.7}N/GaN/Al_{0.04}Ga_{0.96}N$ high electron mobility transistors. Silicon. https://doi.org/10.1007/s12633-020-00899-z
37. Kumar JSR, Nirmal D, Hooda MK, Singh S, Ajayan J, Arivazhagan L (2021) Intensive study of field-plated AlGaN/

GaN HEMT on silicon substrate for high power RF applications. Silicon. https://doi.org/10.1007/s12633-021-01199-w

38. Hamza KHusnaAugustine Fletcher DNirmal,AS (2021) L.Arivazhagan,J.Ajayan,RamkumarNatarajan10.1016/j.aeue.2021.153774Kumar JSR, Nirmal D, Hooda MK, Surider Singh, Ajayan J, Arivazhagan L (2021) Highly scaled graded channel GaN HEMT with peak drain current of 2.48A/mm (2021). AEU- Int J Electron Commun 136:153774. https://doi.org/10.1016/j.aeue.2021.153774

39. Bulutay C (2002) Electron initiated impact ionization in AlGaN alloys. Semicond Sci Technol 17:59–62. https://doi.org/10.1088/0268-1242/17/10/102

Publisher's Note Springer Nature remains neutral with regard to jurisdictional claims in published maps and institutional affiliations.